Magnetic Microbot Design Framework for Antiangiogenic Tumor Therapy

Lyès Mellal, David Folio, Karim Belharet, Antoine Ferreira

Magnetic Microbot Design Framework for Antiangiogenic Tumor Therapy

Lyès Mellal[1], David Folio[1], Karim Belharet[2] and Antoine Ferreira[1]

***Abstract*— This paper presents an optimal design strategy for magnetic targeting of therapeutic drugs. In this study, to maximize the effect of the treatment and minimize adverse effects on the patient, a mathematical model have been developed to find the number and the size of the boluses with respect to the growth of a tumor. Using these models, control strategies are developed to establish a schedule that allows the physician to administer the medication while respecting borne by the patient doses. To transport the drugs, we use therapeutic magnetic boluses composed of magnetic particles aggregates as navigable agents controlled by magnetic gradients. Based on the optimal design of the bolus, an experimental investigation is carried out in millimeter-sized fluidic artery vessels to demonstrate the steerability of the magnetic bolus under different velocity, shear-stress and trajectory constraints with a laminar viscous fluidic environment.**

I. INTRODUCTION

The targeted delivery of nanoparticles to malignant tumors is an important method in the development of cancer nanomedicine [1]. Magnetic targeting is a method that attempts to concentrate navigable micro-entities such as Therapeutic Magnetic Micro Carriers (TMMC) in a targeted site by applying external magnetic fields [2]. The magnetic targeting of deep tissues is highly challenging and is not used in clinical practice [3]. A new approach based on upgrading a typical clinical magnetic resonance scanner with adequate steering coils referred as Magnetic Resonance Navigation (MRN) has been proposed to navigate TMMCs in deep tissues and keep the systemic carrier distribution under control [4], [5]. To benefit both from a large motive force in the macrovasculature and from a possible break up in the microvasculature (so as to avoid undesired thrombosis and to improve the targeting), a promising approach is to consider aggregates. Such aggregates of magnetic microparticles (termed bolus hereafter) are binded either by a biodegradable ligand [6], [7] or by self-assembly properties [8]. Already, polymer particles embedding doxorubicin as a therapeutic agent were successfully synthesised and steered in a rabbit liver using a 400 mT.m^{-1} unidirectional gradient coil [2]. However, as shown in Fig.1(a), several milliliters of therapeutic particles need to be injected in order to reach the required therapeutic drug dose. Navigation of such agents requires the injection of consecutive boluses that will be serially steered from the injection site (the tip of the catheter as shown in Fig.1(b)) to the target location (tumor site as shown in Fig.1(c)) before to break-up into nanometer constituents. Navigation of such agents needs to know precisely the number, size, shape and steering properties of boluses to be injected with respect to the developmental stage of the tumor, its location and accessibility [9].

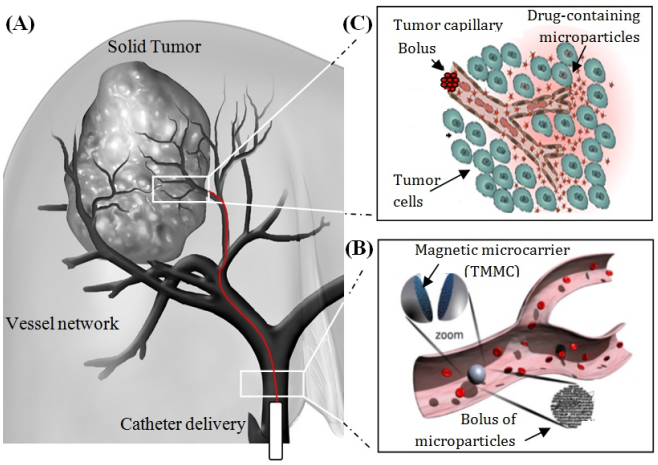

Fig. 1. Inset A represents the vascular network feeding the tumor growth. By correctly applying magnetic gradients, inset B shows that the control of the injected boluses to navigate only toward the disease site (lung carcinoma) preserves healthy tissues. The image zoom illustrates a schematic representation of a cut of the self-assembled magnetic bolus loaded with an antitumor drug and magnetic nanoparticles. Inset C displays the magnetic targeting of the tumor by producing chemoembolization of the multiple capillaries feeding the tumor. The bolus is broken in multiple aggregates creating capillary embolies.

In this study, to maximize the effect of the treatment and minimize adverse effects on the patient, a mathematical model has been developed to find the number and the size of the boluses with respect to the growth of a tumor. Using these models, control strategies are developed to establish a schedule that allows the physician to administer the medication while respecting borne by the patient doses. Furthermore, the aggregation size is the key factor for successful and efficient propulsion within the blood vessels. A relatively large aggregation could form clots in the small arteries or conversely a very small one would be dragged away by the systemic circulation. Based on the optimal design of the bolus, an experimental investigation is carried out in *mm*-sized fluidic artery phantoms to demonstrate the steerability of the magnetic bolus. Different velocity and trajectory constraints are considered under a laminar viscous fluidic environment. The experiments show the feasibility to perform magnetic aggregation and mechanical break-up of boluses constituted

[1]L. Mellal, D. Folio and A. Ferreira are with INSA Centre Val de Loire, Université d'Orléans, PRISME EA 4229, Bourges, France. Corresponding author: Antoine Ferreira (Email: antoine.ferreira@insa-cvl.fr

[1]Karim Belharet is with Hautes Études d'Ingénieur campus Centre, PRISME EA 4229, Châteauroux, France.

of hundreds of superparamagnetic microparticles of 9μm of diameter. This paper consists of four sections. Section II details the need for a tumor growth model in order to estimate the number of boluses that are required for medication. Then, in Section III, the analysis of a bolus aggregate navigating in blood vessel is presented. Section IV is dedicated to the experimental investigation of the steerability of a bolus aggregate and break up under laminar fluid environment. Conclusion and discussions on open issues are summarized in Section V.

II. TUMOR GROWTH MODELING

A. Background

Classically, the tumor growth occurs in three stages. First, an avascular step occurs where the tumor obtains its nutrients from its immediate environment, through the blood vessels. At this stage, the tumor is difficult to detect on medical images. Secondly, the tumor can continue to expand by seeking additional sources of nutrients. At this angiogenesis step, endothelial cells migrate to the tumor, forming new blood vessels. Hence, symptoms may appear and the tumor becomes detectable. Thirdly, the tumor reaches the metastasis stage where it spreads to another part of the body. Several mathematical tumor models have been developed to analyze the tumor growth. These models can be incorporated into a given treatment strategy (such as chemotherapy, immunotherapy, radiotherapy...) or, in some cases, a combination of therapies. For instance, the mathematical model of Stepanova [10] is based on two ordinary differential equation (ODE) describing the interactions between cancer cell growth and the immunological activities. Nevertheless, Stepanova's model, and some of its extensions as in [11], could be used mainly for small cancer volumes. Other theoretical models [12] take into account three populations (e.g. populations of normal cells , of tumor cells and tumor immunity) and serve as an analytical tool for cell growth with or without chemotherapy. Hahnfeldt *et al.* [13] have proposed a theoretical model for the growth of a tumor that has been validated experimentally on mice infected with lung cancer (Lewis lung carcinoma–LLC). Especially, the Hahnfeldt's tumor growth model is built by considering the action of angiogenic inhibition (i.e. limit the growth of new blood cells). Actually, anti-tumor angiogenesis is seen as a therapy for a wide range of cancer, and is not subject to provide drug resistance.

B. Hahnfeldt's Model of Tumor Growth

In this work, we consider the tumor growth formulation from [14] that is based on the previously developed and validated model in [13]. In this Hahnfeldt's model the state representation of the underlying diffusion that stimulate and inhibit angiogenesis are incorporated into a model for cancer cells and vascular endothelial cells. Let p define the volume (in mm^3) of a primary tumor cells, and e denote the volume (in mm^3) of the vascular endothelial cells that supplies the tumor with nutrients. Classically, the growth of a tumor is described by different empirical growth curves, such as exponential [15], Gompertzian [13] or a generalized-logistic law [12]. The Hahnfeldt's model considers that the tumor growth follows a Gompertzian function, and leads to the following nonlinear equation [13]:

$$\dot{p}(t) = -\lambda_p p \ln\left(\frac{p(t)}{e(t)}\right) \quad (1)$$

$$\dot{e}(t) = bp(t) - dp(t)^{2/3}e(t) - ke(t)g(t) \quad (2)$$

$$g(t) = \int_0^t c(\tau)\exp\left(-\lambda_g(t-\tau)\right)d\tau \quad (3)$$

with $g(t)$ the concentration of administered drug inhibitor[1] (conc); and $c(\tau)$ the rate of administration inhibitor concentration (conc/day).

Drexler *et al.* [14] have proposed a modified version of the Hahnfeldt's model (1)-(3) based on the knowledge of clearance of the administered inhibitor. To this aims, the authors consider a Dirac deltas as input $u = c(\tau)$, meaning that the drug was given to the patient in the form of injection. Hence, the tumor kinetic model is then defined by:

$$\dot{p} = -\lambda_p p \ln\left(\frac{p}{e}\right) \quad (4)$$

$$\dot{e} = bp - dp^{2/3}e - keg \quad (5)$$

$$\dot{g} = -\lambda_g g + u \quad (6)$$

where u is the input inhibitor drug administration rate.

1) Tumor Growth Parameters: In the both tumor growth modeling (1)-(3) and (4)-(6), the model constant parameters are defined as:

- λ_p tumor growth rate (/day) ;
- b vascular endothelial cells birth rate (/day);
- d vascular endothelial cells death rate ($/(\text{day}\cdot\text{mm}^{2/3})$);
- k drug killing parameter $/(\text{day}\cdot\text{conc})$);
- λ_g drug clearance rate (/day).

The growth parameters set $\{\lambda_p, b, d\}$ has been identified by Hahnfeldt *et al.* [13] from experimental data made with mice diseased with lung cancer (Lewis lung carcinoma–LLC). In steady-state, the tumor kinetic model converges to the equilibrium $\{p_0, e_0, g_0\}$. In particular, considering the above models and if there are no administered drugs, it is straightforward to demonstrate that:

$$p_0 = e_0 = \left(\frac{b}{d}\right)^{3/2} \quad (7)$$

Hence, the tumor equilibrium is related to the vascular birth and death rate, which depends only on the type of tumor and the patient.

The drug pharmacokinetic parameters set $\{k, \lambda_g\}$ rely on the chosen inhibitor. In antiangiogenic therapy, several angiogenesis inhibitors are currently in preclinical or clinical trials. In particular, endostatin [16] is known as one most efficient inhibitor. Indeed, endostatin inhibits endothelial cell proliferation, angiogenesis and the endogenous angiogenesis inhibitors in the body. Moreover, endostatin has the broadest

[1]The unit of concentration (conc) is measured by the ratio of the mass of the drug and the body mass of the patient in mg/kg.

anti-cancer spectrum. Therefore in this work we focus on endostatin drug inhibitor. The Table I summarize the different parameters set used in this work.

TABLE I
TUMOR GROWTH PARAMETERS

Tumor growth parameters			Drug pharmacokinetic parameters		
λ_p	$0.192/\ln(10)$	(/day)	λ_g	1.7	(/day)
b	0.5; 5.85; 8	(/day)	k	1.7	(/(day · conc))
d	0.00873	(/(day · mm$^{2/3}$))			

2) Model Analysis of Tumor Growth: The open-loop analysis of the tumor kinetic allows us to evaluate the tumor evolution over time. The Fig.2 shows the evolution of a tumor over time. After 120 days, the tumor reached a volume of 433 mm^3, which will correspond to the avascular phase (blue line in Fig.2). Without applying any treatment, the tumor continues to grow to a volume of 17347 mm^3 until reaching the vascular phase (green curve in Fig.2). One can notice that the tumor and the endothelial volume increased rapidly during the first 60 days through a Gompertzian curve. This increase is due to the strong presence of nutrients carried by the endothelial cells, that feed the tumor. That is why the endothelial volume growths faster compared to the tumor volume. Thus, if the rate of vascular birth b increases, the tumor volume is then 27415 mm^3, and it may reach the metastases phase.

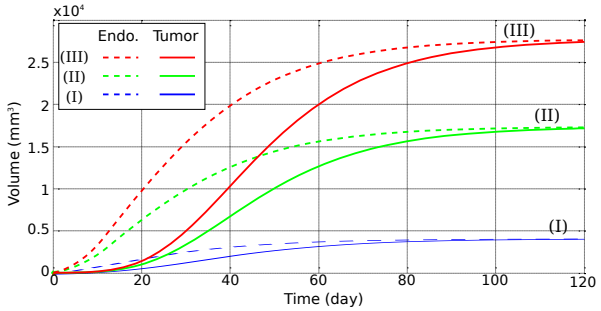

Fig. 2. Evolution of the tumor (plain line) and endothelial (dashed line) volumes in avascular (blue), vascular (green) and metastasis (red) stages.

C. Optimal Control of Input Drug

Optimal control techniques have been applied in the context of cancer immune-interactions [12] or antiangiogenic therapy [14] to define the optimal treatment and drug dose. Especially, the motivation is to reduce the volume of the tumor while avoiding the toxicity of the human body by the high doses of the drug to be administered. To solve this optimization problem a solution is to use a linear-quadratic regulator (LQR) design [17]. Let us consider the nonlinear system dynamics (4)-(6) which could be linearized as:

$$\dot{x} = Ax + Bu, \quad \text{with} \quad x = (p,e,g)^T \tag{8}$$

Hence, the following quadratic cost function is proposed to reduce the volume of the tumor and the drug concentration in the blood [14]:

$$J(t,x) = \int_0^\infty \{x^T(t)Qx(t) + u^T(t)Ru(t)\}dt \tag{9}$$

with:

$$R = 10^5, \quad \text{and} \quad Q = \begin{bmatrix} 1 & 0 & 0 \\ 0 & 0 & 0 \\ 0 & 0 & 1 \end{bmatrix} \tag{10}$$

The Q and R values are chosen to take into account the volume of the tumor and the drug concentration, while preventing the high doses. The feedback control law that minimize the criterion (9) is then classically given by:

$$u(t) = -Kx(t) \tag{11}$$

where $K = -R^{-1}B^TP$, with P the solution of the well known continuous time algebraic Riccati equation (CARE):

$$PA + A^TP - PBR^{-1}B^TP + Q = 0 \tag{12}$$

and the matrix A and B are obtained using the following method. First, in the growth modeling (4)-(6), the model will be rewritten as:

$$\dot{x} = f(w) + g(x)u, \quad \text{with} \quad x = (p,e,g)^T \tag{13}$$

$$y = p \tag{14}$$

where

$$f(x) = \begin{bmatrix} -\lambda_1 p \ln(\frac{p}{e}) \\ bp - dp^{2/3}e - keg \\ -\lambda_3 g \end{bmatrix} \quad \text{and} \quad g(x) = \begin{bmatrix} 0 \\ 0 \\ 1 \end{bmatrix} \tag{15}$$

The model will be then linearized around the operating point which varies instantaneously, by calculating the Jacobian matrix $J = \frac{\partial f(x)}{\partial x}$ defined as:

$$J = \begin{bmatrix} -\lambda_1 \ln(\frac{p}{e}) - \lambda_1 & \lambda_1 \frac{p}{e} & 0 \\ b - \frac{2}{3}dp^{-2/3}e & -(dp^{2/3} + kg) & -ke \\ 0 & 0 & -\lambda_3 \end{bmatrix} \tag{16}$$

Thus, the linear model is in the following form

$$A = \begin{bmatrix} -\lambda_1 \ln(\frac{p}{e}) - \lambda_1 & \lambda_1 \frac{p}{e} & 0 \\ b - \frac{2}{3}dp^{-2/3}e & -(dp^{2/3} + eg) & -ee \\ 0 & 0 & -\lambda_3 \end{bmatrix}, \quad B = \begin{bmatrix} 0 \\ 0 \\ 1 \end{bmatrix} \tag{17}$$

$$C = \begin{bmatrix} 1 & 0 & 0 \end{bmatrix}, D = 0 \tag{18}$$

The proposed linear model is used to apply the linear quadratic control and to limit the amount of drug, the control input u is saturated to an upper limit $u_{\max}$.

Fig.3 illustrates the tumor behavior when an optimal intake of endostatin inhibitor is administered. As one can see, the tumor and the endothelial volumes vanish in about 60 days for the avascular and 40 days for the vascular growth. The corresponding administered dose of drug is depicted in Fig.4. The endostatin has to be injected in two phases. First, the control input u is saturated to i) $u_{\max,1} = 2\,\text{conc/day}$ for the avascular growth; ii) $u_{\max,2} = 79\,\text{conc/day}$ for the vascular growth; and iii) $u_{\max,3} = 90\,\text{conc/day}$ for the metastases stage. The control input is then reduced in

the avascular growth, vascular growth, metastases stage, to about 1 conc/day, 14 conc/day and 20 conc/day respectively, when the volume of the tumor remains close to 0. For instance, a patient with a weight of 60 kg, the applicable daily dose (DD) is given by $\mathrm{DD} = 60 \cdot u$ (mg/day). The Fig.4 shows also the scaling of the posology of injected endostatin in the different phases of growth. Based on this optimal drug delivery synthesis, the following section investigates the feasibility of administrating such treatment using magnetic bolus.

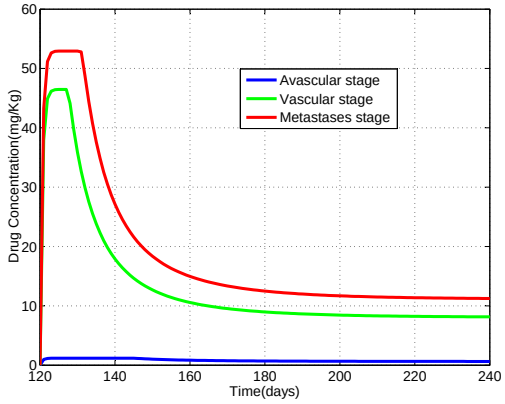

(a)

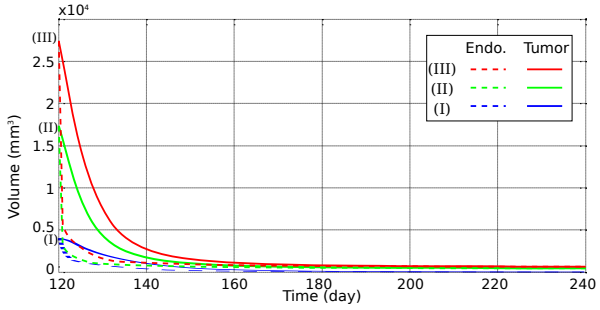

(b)

Fig. 3. Optimal treatment of a tumor: (a) the optimal drug concentration; (b) the corresponding tumor and endothelial decreasing volumes, for avascular (blue), vascular (green) and metastases stage.

III. MICROPARTICLE AGGREGATIONS FOR OPTIMAL DRUG DELIVERY

To transport the therapeutic drugs, we consider hereafter superparamagnetic iron oxide microparticles (BioMag BM547, Bang Laboratories, Inc.). The microparticles have a diameter in the range $\sim 9\,\mu$m embedding therapeutic agents. Although the saturation magnetization of iron oxide is not optimal ($M_{\mathrm{sat}} = 35\,\mathrm{emu/g}$), it is still acceptable with the advantage to being widely used clinically. However, to be used as therapeutic agents, their very low value of magnetic material results in very high gradients fields that limit their application with MRI-guided delivery. To increase the effective volume of magnetic material, novel approaches use self-assembled aggregates (dipole-dipole interactions) of particles [8] or biodegradable polymer [2] to form large

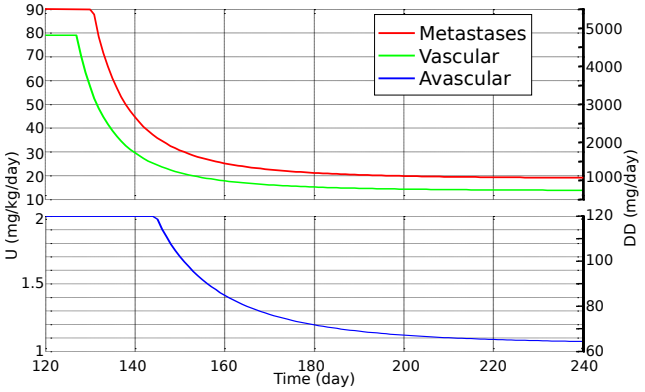

Fig. 4. Evolution of the drug uptake over time (left y-axis) and the corresponding drug amount applied for a patient with a weight of 60 kg (right y-axis).

bolus of aggregates. In order to optimize the magnetic force being induced, the effective volume should be optimized with respect to the narrowed vessels in the tumor site, the quantity of drugs, the number of bolus and the MRI actuation limitations. In the following, we consider that the bolus is magnetically actuated thanks to a magnetic gradient of $\nabla \mathbf{b} = 80\,\mathrm{mT/m}$ generated from a MRI scanner.

To be controllable, the bolus should have its optimal non-dimensional magnetophoretic number C_{mt} ratio greater than 1 [9]. This magnetophoretic number, introduced in [18], is defined as follows:

$$C_{mt} = \frac{\mathbf{f}_{\mathrm{m}}}{\mathbf{f}_{tot}} = \frac{\mathbf{f}_{\mathrm{m}}}{\mathbf{f}_{\mathrm{d}} + \mathbf{f}_{w} + \mathbf{f}_{el} + \mathbf{f}_{vdw}} \tag{19}$$

The terms $\mathbf{f}_{\mathrm{m}}$, $\mathbf{f}_{\mathrm{d}}$, $\mathbf{f}_{w}$, $\mathbf{f}_{el}$ and $\mathbf{f}_{vdw}$ are respectively the magnetic gradient, the drag, the apparent weight, the electrostatic, and the van der Waals forces (for detailed expression of these microforces see [19]). As shown in Fig. 5, the optimal ratio is given for the following characteristics: a bolus with a radius of $r = 250\,\mu$m and a minimum magnetization rate of 46%.

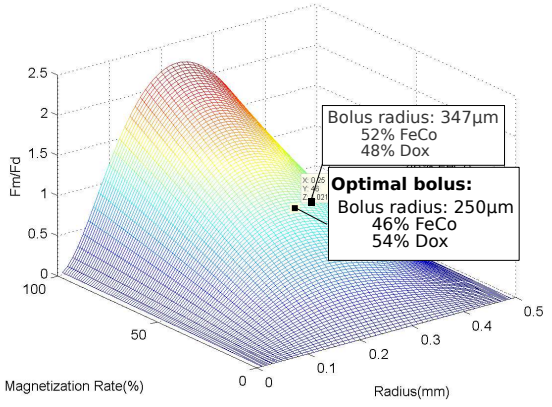

Fig. 5. Ratio driving force ($\mathbf{f}_{\mathrm{m}}$)/drag force ($\mathbf{f}_{\mathrm{d}}$) as function of radius and magnetization rate (%).

To calculate the number of boluses needed to transport the amount of drug obtained in Section II, it is necessary to calculate the overall mass of the bolus. Obviously, the

mass is retrieved from its volume and density. The average number of boluses is then calculated using $N_b = \frac{DD}{m_d}$ leading to a number of magnetic particles at a concentration of 0.78×10^5 particles per ml. The Fig.6 and the Fig.6 represent the evolution of the bolus and particles number over time in different phases of growth, during the first 20 days of treatment. It can be noticed that the maximal number of boluses needed is i) 720 in the avascular growth, ii) 2.80×10^3) in the vascular growth, and iii) 3.25×10^3 in the metastases stage. The corresponding drug volume are 120 mg, 4775 mg and 5450 mg. It can be seen that the number of bolus decreases gradually over time to a value of 400, 5000 and 7000 boluses corresponding to a concentration of 3×10^7, 0.35×10^9 and 0.55×10^9 of particles.

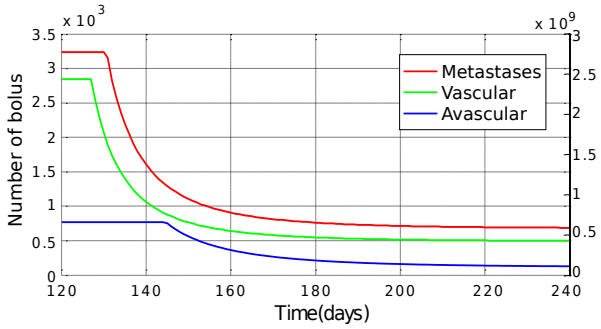

Fig. 6. Evolution of boluses number over time with the corresponding number of SPIO particles.

IV. RESULTS

A. Experimental Setup

To validate experimentally the findings of model simulations, an experimental setup has been specifically developed by Aeon Scientific. The system consists of three nested sets of Maxwell coils and one nested set of Helmholtz coils [20], and is illustrated in Fig.7(a). Such arrangement allows generating a constant-gradient magnetic field pointing in x, y, and z-axis direction. The generated magnetic gradient is saturated to $\nabla \mathbf{b}_{\max} = 40\,\mathrm{mT/m}$ to be compatible with clinical MRI scanner. Magnetic gradient forces will thus be exerted on the bolus that is placed inside a microfluidic chip Fig.7(b). An aqueous solution of 50% water–50% glycerol is pumped using a pulsatile pump (Harvard Apparatus), and the microcircuits enable the hepatic artery mimicking. Droplets containing superparamagnetic iron oxide (SPIO) particles (BioMag BM547, Bang Laboratories, Inc.) are injected through a controlled syringe pump in the injection input via a flexible microcatheter.

B. Navigation in cylindrical microchannel

First, the navigation behavior of a single bolus of radius $r = 347.5\,\mu\mathrm{m}$ in a microfluidic ship with variable section is investigated. For such bolus size the optimal magnetization rate is about 52% that allows carrying $0.084\,\mathrm{mm}^3$ of drug load (see also Fig. 5). Fig. 8 shows the bolus navigation evolution which traveled 11.57 mm in about 1 s. Especially,

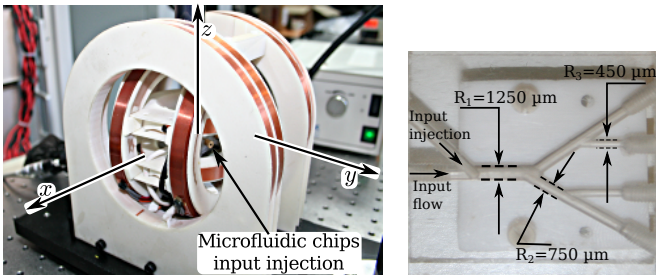

(a) (b)

Fig. 7. Experimental setup: (a) 3D Maxwell-Helmholtz coils and (b) a W-shaped microfluidic arterial bifurcation chip.

with a flow rate of $Q = 3.33\,\mathrm{ml/s}$, the bolus experiences different dynamics, as illustrated with its velocity in Fig. 9.

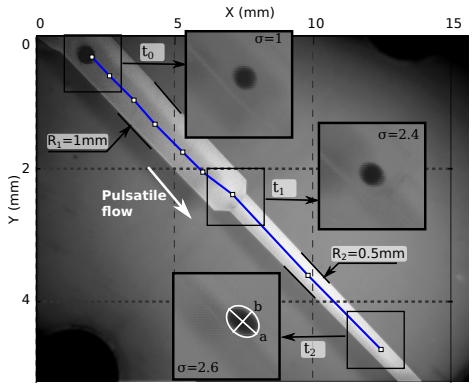

(a)

Fig. 8. Magnetic bolus navigating in a cylindrical channel with different radius.

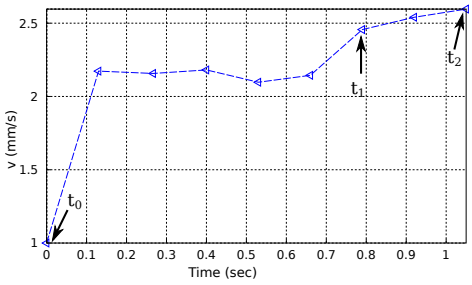

Fig. 9. Magnetic bolus velocity.

Furthermore, microaggregates of SPIO particles with polymeric solutions demonstrate stability in aqueous solutions due to their hydrophobicity. The bolus start with a spherical shape (inlet t_0 in Fig. 8) of radius $r = 347.5\,\mu\mathrm{m}$. While the shear stress is increasing, the shape became more ellipsoidal-like (inlet t_1-t_2 in Fig. 8). Hence, the aspect ration $\sigma = a/b$ (with a the major and b the minor axis) of the magnetic microrobot evolves during the navigation in thin vessel. Fig. 10 illustrates the influence of the vessel radii variation on the bolus shape. We see clearly that the bolus is exposed to hemodynamic shear stresses that disturb the attractive forces holding the microparticles together. To determine the shear-

sensitivity of the microparticle deployment mechanism, we estimated from calculation the shear-stress for a cylindrical vessel as:

$$\tau_w = -\eta Q \frac{(R-\delta)}{R^3} \tag{20}$$

with Q the volumetric flow rate, η the fluid viscosity, R the microchannel radius, δ the distance to the wall. The experimental results given in Fig. 10 demonstrates the great influence of the shear-stress mechanism on the shape of the aggregate, and probably on its break-up.

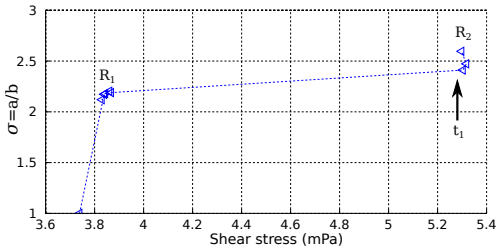

Fig. 10. Aspect ratio $\sigma = a/b$ (with a the major and b the minor axis of the ellipse) as function of the shear stress τ_w.

C. Navigation in W-shaped microchannel

The experiments are then carried out in a W-shaped microfluidic to consider environment with complex bifurcations. Fig. 11 shows a typical bolus navigation results with its associated magnetic gradient $\nabla \mathbf{b}$. This result demonstrated the feasibility to drive efficiently bolus even with multiple bifurcations. Let us notice that the motion of the bolus is in the same order of magnitude as those previously observed in paragraph IV-B. Thus, this suggests that about 1800 boluses could be conveyed in 30 min, and an amount of drug of 1537.7 mg administered.

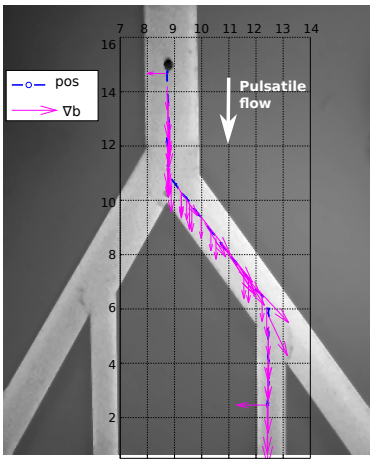

Fig. 11. Magnetic navigation control of bolus in W-shaped microchannel.

However, the experiments shows that the bolus must navigate close to the vessel centerline to avoid its break up. Actually, the wall shear stress could induce a mechanical forces that overcome the attractive forces holding the microparticles together, as depicted in Fig. 12.

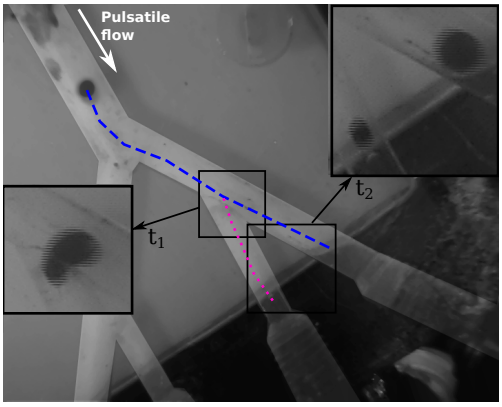

Fig. 12. The wall shear stress induces a bolus splitting in the vicinity of a bifurcation.

V. Conclusion

The paper described an optimal design strategy for magnetic targeting of therapeutic drugs using magnetic microparticle aggregates. To propel these aggregations through the arteries ($\sim$ 5mm) and small arteries ($\sim$ 500 μm) down to the thinner blood vessels that surround the tumor requires important magnetic gradients leading to large boluses of agglomerates. That is why, to maximize the effect of the treatment and minimize adverse effects on the patient, a mathematical model have been developed to find the number and the size of the boluses with respect to the growth of a tumor. Using these models, the preliminary results demonstrate that boluses of aggregates can be navigated though phantoms-like arteries to initiate drug targeting. Future work will consider the navigation in a clinical MRI a using various sizes of aggregates delivered through a microcatheter.

References

[1] S. Nie, Y. Xing, G. J. Kim, and J. W. Simons, "Nanotechnology applications in cancer," *Annu. Rev. Biomed. Eng.*, no. 9, pp. 257–288, 2007.

[2] P. Pouponneau, J.-C. Leroux, G. Soulez, L. Gaboury, and S. Martel, "Co-encapsulation of magnetic nanoparticles and doxorubicin into biodegradable microcarriers for deep tissue targeting by vascular mri navigation," *Biomaterials*, no. 32, pp. 3481–3486, 2011.

[3] C. Alexiou, R. Tietze, E. Schreiber, R. Jurgons, H. Richter, L. Trahms, H. Rahn, S. Odenbach, and S. Lyer, "Cancer therapy with drug loaded magnetic nanoparticles-magnetic drug targeting," *Journal of Magnetism and Magnetic Materials*, no. 323, pp. 1404–1407, 2011.

[4] J. B. Mathieu and S. Martel, "Magnetic microparticle steering within the constraints of an mri system: proof of concept of a novel targeting approach," *Biomedical microdevices*, no. 9, pp. 801–808, 2007.

[5] P. Pouponneau, J. C. Leroux, and S. Martel, "Magnetic nanoparticles encapsulated into biodegradable microparticles steered with an upgraded magnetic resonance imaging system for tumor chemoembolization," *Biomaterials*, no. 30, pp. 6327–6332, 2009.

[6] N. Korin, M. Kanapathipillai, B. Matthews, M. Crescente, A. Brill, T. Mammoto, K. Ghosh, S. Jurek, S. Bencherif, D. Bhatta, A. Coskun, C. Feldman, D. Wagner, and D. Ingber, "Shear-activated nanotherapeutics for drug targeting to obstructed blood vessels," *Science*, no. 337, pp. 6738–6742, 2012.

[7] B. Morgan, A. Kennedy, V. Lewington, B. Jones, and R. Sharma, "Intra-arterial brachytherapy of hepatic maliggnancies : watch the flow," *Nature Reviews: Clinical oncology*, no. 8, pp. 115–120, 2011.

[8] P. Vartholomeos and C. Mavroidis, "In silico studies of magnetic microparticle aggregations in fluid environments for mri-guided drug delivery," *IEEE Transactions on Biomedical Engineering*, vol. 11, no. 59, pp. 3028–3038, 2012.

[9] L. Mellal, K. Belharet, D. Folio, and A. Ferreira, "Optimal structure of particles-based superparamagnetic microrobots: application to MRI guided targeted drug therapy," *J. of Nanoparticle Research*, vol. 17, no. 2, pp. 1–18, 2015.

[10] N. Stepanova, "Course of the immune reaction during th e development of a malignant tumour," *Biophysics*, no. 24, pp. 917–923, 1980.

[11] V. A. Kuznetsov, I. A. Makalkin, M. A. Taylor, and A. S. Perelson, "Nonlinear dynamics of immunogenic tumors: Parameter estimation and global bifurcation analysis," *Bulletin of Mathematical Biology*, vol. 56, no. 2, pp. 295–321, 1994.

[12] L. D. Pillis and A. Radunskaya, "The dynamics of an optimally controlled tumor model: A case study," *Mathematical and Computer Modelling*, vol. 37, no. 11, pp. 1221–1244, 2003, modeling and Simulation of Tumor Development, Treatment, and Control.

[13] P. Hahnfeldt, D. Panigrahy, J. Folkman, and L. Hlatky, "Tumor development under angiogenic signaling a dynamical theory of tumor growth, treatment response, and postvascular dormancy," *Cancer research*, vol. 59, no. 19, pp. 4770–4775, 1999.

[14] D. A. Drexler, L. Kovacs, J. Sápi, I. Harmati, and Z. Benyo, "Model-based analysis and synthesis of tumor growth under angiogenic inhibition: A case study," in *IFAC World Congress*, vol. 18, no. 1, 2011, pp. 3753–3758.

[15] Y. Zheng, H. Moore, A. Piryatinska, T. Solis, and E. A. Sweet-Cordero, "Mathematical modeling of tumor cell proliferation kinetics and label retention in a mouse model of lung cancer," *Cancer research*, vol. 73, no. 12, pp. 3525–3533, 2013.

[16] M. S. O'Reilly, T. Boehm, Y. Shing, N. Fukai, G. Vasios, W. S. Lane, E. Flynn, J. R. Birkhead, B. R. Olsen, and J. Folkman, "Endostatin: an endogenous inhibitor of angiogenesis and tumor growth," *cell*, vol. 88, no. 2, pp. 277–285, 1997.

[17] K. Zhou, J. C. Doyle, K. Glover *et al.*, *Robust and optimal control*. Prentice Hall New Jersey, 1996, vol. 40.

[18] J.-B. Mathieu, G. Beaudoin, and S. Martel, "Method of propulsion of a ferromagnetic core in the cardiovascular system through magnetic gradients generated by an mri system," *IEEE Trans. Biomed. Eng.*, vol. 53, no. 2, pp. 292–299, 2006.

[19] A. F. Laurent Arcese, Matthieu Fruchard, "Endovascular magnetically guided robots: Navigation modeling and optimisation," *IEEE Trans. Biomed. Eng.*, vol. 59, no. 4, pp. 977–987, 2012.

[20] K. Belharet, D. Folio, and A. Ferreira, "Control of a magnetic microrobot navigating in microfluidic arterial bifurcations through pulsatile and viscous flow," in *IEEE/RSJ Int. Conf. on Intell. Robots and Syst. (IROS)*. IEEE, 2012, pp. 2559–2564.